J. At. Mol. Sci.
doi: 10.4208/jams.041313.062213a

Vol. **5**, No. 1, pp. 64-80
February 2014

Pressure induced phase transition and superconducting properties of PtH and IrH: a first principles study

G. Sudhapriyanga[a], A. T. Asvinimeenaatci[a], R. Rajeswarapalanichamy[a,*], and K. Iyakutti[b]

[a] *Department of Physics, N.M.S.S. Vellaichamy Nadar College, Madurai, Tamilnadu-625019, India*
[b] *Department of Physics & Nanotechnology, SRM University, Chennai, Tamilnadu-603203, India*

Received 13 April 2013; Accepted (in revised version) 22 June 2013
Published Online 18 November 2013

Abstract. The electronic, structural, mechanical and superconducting properties of PtH and IrH are investigated using first principles calculation based on density functional theory with generalized gradient approximation. The calculated lattice constants at normal pressure are in good agreement with experimental and other theoretical results. Among the five crystallographic proposed structures investigated, the cubic phase is found to be more stable than the hexagonal ones. A new high pressure CsCl phase is predicted for Iridium hydride. The maximum superconducting transition temperature achieved in Platinum hydride and Iridium hydride are 23.8K and 10K respectively. The calculated elastic constants indicate that both the hydrides are mechanically stable at ambient pressure.

PACS: 61.50.Ks, 31.15.A-, 62.20.-x, 74.20.pq

Key words: structural phase transition, electronic structure, elastic properties, superconducting transition temperature

1 Introduction

Density functional theory (DFT) calculations of metal- hydrogen systems represent a growing field of research [1]. Hydrogen is known to form compounds with many elements in the periodic table [2]. Among those, the metal hydrides are of particular interest due to their application in hydrogen storage for fuel cells [3, 4] or heat storage for the solar-energy industry [5]. Platinum (Pt) and Iridium (Ir) are frequently used to form electrodes (which allow measurements of electrical resistance, the concentration of electrical

*Corresponding author. *Email address:* rajeswarapalanichamy@gmail.com (R. Rajeswarapalanichamy)

carriers and the Hall mobility) and as heat coupler. Pt and Ir play a very important role in high pressure studies [6-8]. Although a number of transition metal hydrides have been synthesized under high pressure conditions [9], the investigation of platinum hydride (PtH) and iridium hydride (IrH) is rare especially in its high pressure behavior. There are only a few works on high pressure study of platinum hydride [10-13] and there are no experimental and theoretical investigations on the structural phase transition of IrH. Experimentally Thomas Scheler et.al [14] found two hexagonal phases of PtH, one is stable at low pressure and another predicted P63/mmc structure appears as a single phase of PtH above 42 GPa. Theoretically Papaconstantopoulos et al. [15] has showed NaCl PtH is stable at ambient pressure. Duck Young Kim et al. [16] investigated the superconducting properties of some transition metal hydrides TMH (TM=Rh, Pd, Ag, Pt, Ir and Au) and observed high superconducting transition temperature in fcc phase of platinum hydride (T_c=24.5 K). Still there is a contradiction about the stable structure of Platinum hydride. This motivated us to analyze the structural stability of platinum hydride. Moreover, to the best of our knowledge the structural phase transition and pressure dependence of superconductivity in Iridium hydride have not been reported yet. In the present paper the electronic and elastic properties of PtH and IrH are analyzed under normal pressure. Also a pressure induced structural phase transition and superconducting properties of PtH and IrH are investigated.

2 Computational details

The DFT calculations are carried out using the Vienna ab initio simulation package (VASP) [17-19]. The generalized gradient approximation (GGA) is used for the correlation energy functional with the Perdew-Burke-Ernzehof functional (PBE) [20-21]. In the present computation, the hydrides are assumed to be defect free and the stoichiometric composition for all the hydrides is taken as 1:1 ratio of metal and hydrogen atom. The electronic wave functions are expanded in a plane wave basis set with an energy cut-off of 500 eV and 600 eV for PtH and IrH respectively. To predict the stable structure of PtH and IrH, five possible phases are considered. The space group and atomic positions are tabulated in Table 1.

The valence electron configuration for H, Pt and Ir atoms are $1s^1$, $6s^1$ $5d^9$ and $6s^2$ $5d^7$ respectively. For both PtH and IrH, relaxations are performed so that the convergence of Hellmann-Feynman forces is better than 1 meV/Å. The self-consistent total energy is converged with energy difference less than 0.01 meV. A dense grid of k points in the irreducible wedge of Brillouin zone is used with the sampling generated by the Monkhorst-pack procedure [22]. The Crystalline structure, k-point set, energy cut-off and smearing width of PtH and IrH are given in Table 2.The density of states (DOS) are obtained using the linear tetrahedron method with Blöchl corrections on the relaxed structures.

The tight binding linear muffin tin orbital method [23-27] is used for the estimation of electron-phonon coupling constant and electron-electron interaction parameter. This

Table 1: Space group and atomic position of PtH and IrH with five different phases.

Compound	Phase	Space group	Atomic position
PtH	NaCl	$Fm\bar{3}m$	Pt (0.000, 0.000, 0.000) H (0.500, 0.500, 0.500)
	CsCl	$Pm\bar{3}m$	Pt (0.000, 0.000, 0.000) H (0.500, 0.500, 0.500)
	NiAs	$P6_3/mmc$	Pt (0.000, 0.000, 0.000) H (0.250, 0.250, 0.250)
	Tetragonal	$P6_4/nmm$	Pt (0.250, 0.250, 0.270) H (0.250, 0.750, 0.000)
	Tetragonal	$I\bar{4}m2$	Pt (0.000, 0.000, 0.000) H (0.500, 0.000, 0.250)
IrH	NaCl	$Fm\bar{3}m$	Ir (0.000, 0.000, 0.000) H (0.500, 0.500, 0.500)
	CsCl	$Pm\bar{3}m$	Ir (0.000, 0.000, 0.000) H (0.500, 0.500, 0.500)
	NiAs	$P6_3/mmc$	Ir (0.000, 0.000, 0.000) H (0.250, 0.250, 0.250)
	ZB	$F\bar{4}3m$	Ir (0.000, 0.000, 0.000) H (0.666, 0.333, 0.250)
	WC	$P\bar{6}m2$	Ir (0.000, 0.000, 0.000) H (0.666, 0.333, 0.500)

Table 2: Crystalline structure, k-point set, energy cutoff and smearing width of PtH and IrH.

Element	Structure	k-point set	Energy cutoff (eV)	Smearing width (eV)
PtH	NaCl	$12\times12\times12$	500	0.1
	CsCl	$12\times12\times12$	500	0.1
	Tetragonal	$12\times12\times12$	500	0.1
	Tetragonal	$12\times12\times12$	500	0.1
	NiAs	$12\times12\times12$	500	0.1
ItH	NaCl	$12\times12\times12$	600	0.1
	CsCl	$12\times12\times12$	600	0.1
	ZB	$12\times12\times12$	600	0.1
	WC	$12\times12\times12$	600	0.1
	NiAs	$12\times12\times12$	600	0.1

method treats the one electron potential in relativistic form. In the LMTO scheme the crystal potential is approximated by a series of non-overlapping atomic like potential and a constant potential (muffin tin potential) between spheres. The Schrodinger equation can be solved in these regions. These solutions are then matched at the sphere boundaries

to produce muffin tin orbital. This muffin tin orbital is used to construct a basis which is linear order in energy and rapidly convergent. The exchange correlation potential within the local density approximation is calculated using the parameterization scheme of Von Barth and Hedin. The Wigner-Seitz sphere is chosen in such a way that the boundary potential is minimum and the charge flow between the atoms is in accordance with the electro-negativity criteria. The E and K convergence is also checked. The tetrahedron method [28] of Birllouin zone integration is used to calculate the total density of states.

3 Results and discussion

3.1 Structural stability and ground state properties

The stability of platinum and iridium hydrides are analyzed by calculating the total energy using VASP code based on density functional theory. From the computed total energy, it is found that both PtH and IrH are energetically stable in the rock salt (NaCl) structure. The formation energy of a specific compound is defined as the difference between the total energy of the compound and of its constituent elements. The composition reaction of PtH and IrH is as follows

$$M+\frac{1}{2}H_2 \rightarrow MH, \tag{1}$$

this yields the following expression for the formation energy

$$E_f(MH) = E(MH) - (E_M + \frac{1}{2}E_{H2}) \tag{2}$$

The formation energy E_f is calculated using equation (2) by the total energy of MH, M and H_2 dimer. The calculated formation energy is given in Table 3. From Table 3, it is observed that both PtH and IrH are highly stable in the rock salt (NaCl) structure at ambient pressure. Valence electron density (VED) is defined as the total number of valence electrons divided by volume per unit cell which is an important factor for analyzing the super hard materials. The optimized equilibrium lattice constant a (Å) and c (Å), cell volume V_0(Å^3), valence electron density ρ(electrons/ Å^3) and bond length M-H (Å) for five different phases of PtH and IrH, along with available experimental and other theoretical values [14-16] are given in Table 3.

The calculated lattice constant (a) of both PtH and IrH with NaCl structure at ambient pressure is in agreement with the previous theoretical result quoted in ref. [15, 16]. From Table 3, it is found that the lattice constant a and c of high pressure phase of hexagonal PtH (NiAs structure) and tetragonal PtH (P4/nmm) are in good agreement with the experimental results [14] and [16] respectively. For the IrH, in the WC and NiAs structures, the calculated values of c/a obtained for the relaxed structure is close to its ideal value of $\sqrt{\frac{8}{3}}$. The calculated VEDs of all proposed structures of PtH and IrH are higher than that of individual metals Pt (0.4566) and Ir (0.4838), which is comparable to diamond [29]. It is due to the addition of hydrogen atom to the metal.

Table 3: Calculated lattice parameters a, c (Å), equilibrium volume V_0 (Å^3), valence electron density VED ρ (electrons/ Å^3), formation energy E_f (MH) (eV) and bond length M-H (Å) for the PtH and IrH for five different structures.

Element	Space group	lattice constant (Å)	V_0 (Å^3)	ρ (electrons/Å^3)	M-H (Å)	E_f (eV)
PtH	$Fm\bar{3}m$	$a=b=c=3.952$ $a=b=c=4.105$ [15]	14.29	0.7857	1.96	-4.6819
	$Pm\bar{3}m$	a=b=c=2.683	19.33	0.6789	2.21	-3.8087
	$P6_3/mmc$	$a=b=2.569$; $c=4.3034$ $a=2.779$; $c=4.731$ [14]	22.52	0.4983	2.24	-4.2009
	$P4/nmm$	$a=b=3.399$; $c=2.751$ $a=3.387$; $c=2.851$ [16]	21.69	0.5500	2.19	-1.7989
	$I\bar{4}m2$	$a=b=3.847$; $c=3.059$	18.63	0.6111	2.05	-2.4332
IrH	$Fm\bar{3}m$	$a=b=c=4.165$ $a=b=c=3.88$ [16]	18.07	0.5523	1.66	-4.5477
	$Pm\bar{3}m$	$a=b=c=2.699$	19.68	0.5263	1.57	-3.2955
	$P6_3/mmc$	$a=b=2.55$; $c=4.284$	20.26	0.5039	1.74	-4.3647
	$P\bar{4}3m$	$a=b=c=4.109$	17.29	0.5882	1.91	-2.8697
	$P\bar{6}m2$	$a=b=2.409$; $c=2.891$	15.59	0.6410	1.60	-3.8250

3.2 Electronic properties

Band dispersion along high symmetry lines of PtH and IrH under normal pressure is given in Fig. 1 (a-b).

From Fig. 1(a-b), it is observed that both PtH and IrH exhibit metallic character and their valence bands split into two parts. The lower part of the valence band is dominated by the s state electrons of the metal atoms and slightly influenced by 1s state of the hydrogen atom , while the upper one is a result of strong hybridization from the d state

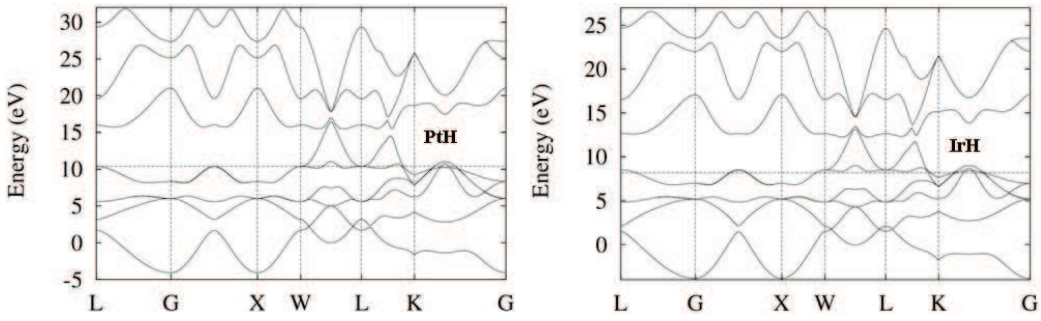

Figure 1: (a)Electronic band structure of PtH; (b)Electronic band structure of IrH.

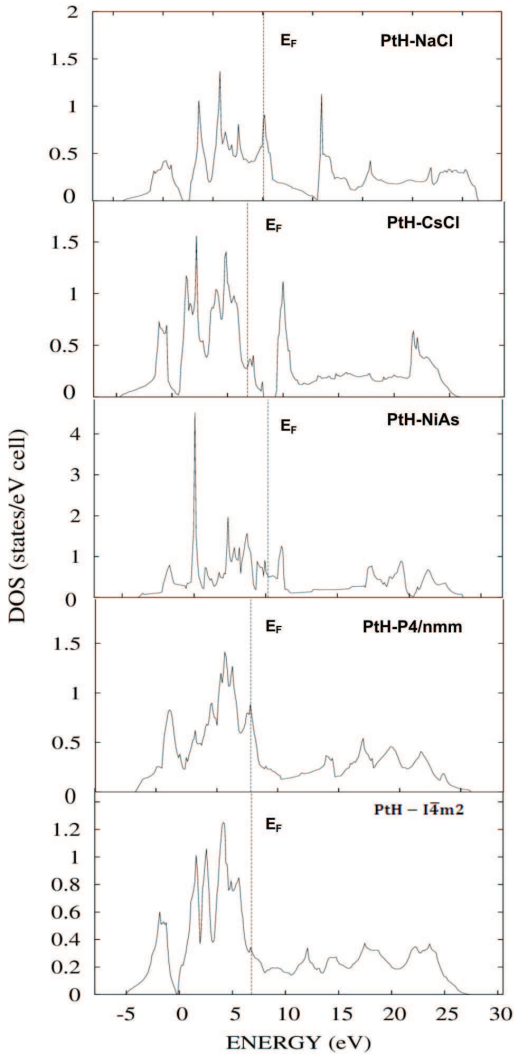

Figure 2: Total density of states (DOS) of PtH with five different structures.

electrons of metal atoms (Pt, Ir) and the 1s state of H atom. Above the Fermi level the empty conduction bands are present with a mixed s, p and d characters.

Figs. 2 and 3 shows total density of states (DOS) for five different structures of PtH and IrH under ambient condition respectively. For PtH and IrH in the NaCl structure, a deep valley called the pseudo gap is found near the Fermi level, which results from the strong hybridization between metal (Pt, Ir) 5d states and hydrogen (H) 1s state and also indicates the significant covalent bonding. For PtH and IrH in the CsCl structure, the energy region for the hybridization between metal (Pt,Ir) 5d states and hydrogen (H) 1s state is from -5 eV to 5 eV.

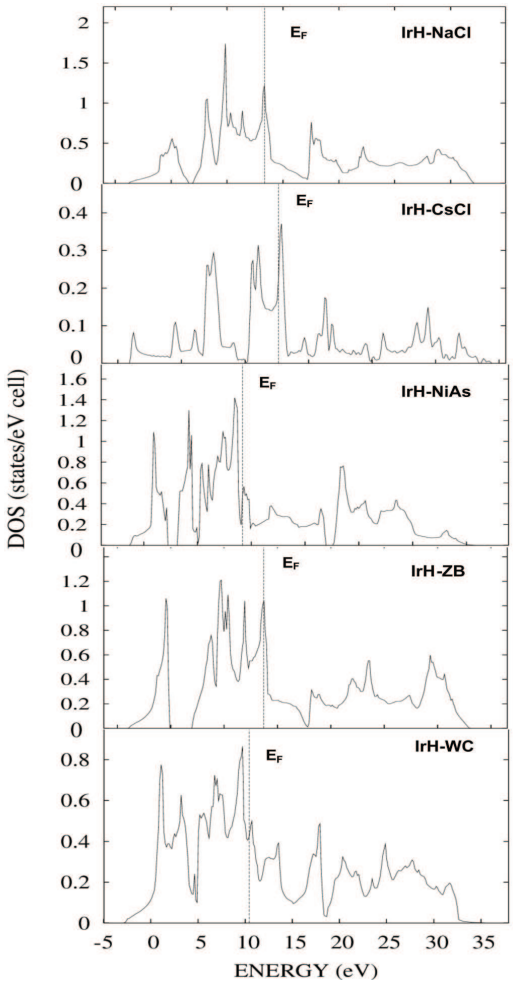

Figure 3: Total density of states (DOS) of IrH with different structures.

For the PtH, the main peak appears at the energy region 0 eV to 5 eV is due to Pt 5d state electrons in both tetragonal structures. The peaks appear at 10 eV in the ZB structure is dominated by the 5d states of Ir atom. For PtH and IrH in the NiAs structure, the peaks from -5 eV to 0 eV are mainly due to the 5d states of metal atoms and 1s states of hydrogen atoms which exhibits a strong hybridization. The DOS around the Fermi energy level of both PtH and IrH in the NaCl structure is much higher than that in the other structures, indicating PtH and IrH in the NaCl structure has higher conductivity. To further investigate the metallic properties of PtH and IrH, the projected density of states (PDOS) are shown in Fig. 4 (a) and (b) for the NaCl phase.

Interestingly, for both the compounds, the metal 5d state electrons dominate the energy range of -5 eV below the Fermi level, and there is a strong hybridization between metal 5d and H 1s electrons in the energy range from -10 eV to 5 eV. For the PtH (Fig.

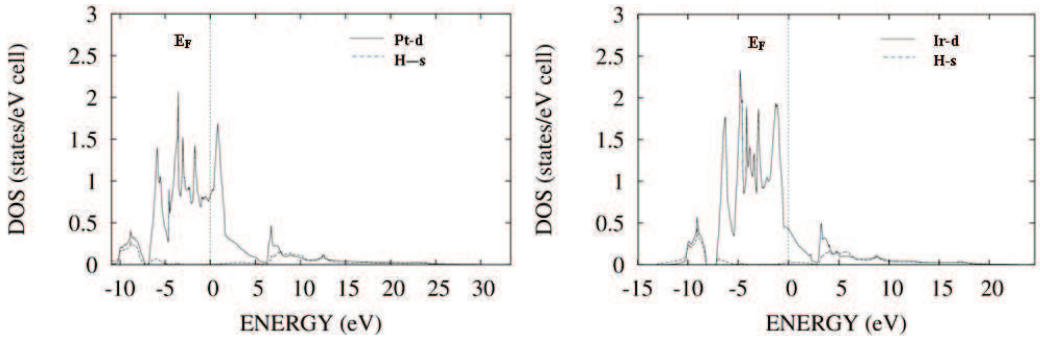

Figure 4: (a)Partial density of states (PDOS) of PtH; (b)Partial density of states (PDOS) of IrH.

2) and IrH (Fig. 3) in the NaCl phase, the highest peak below the Fermi level (at 5 eV) is due to the 5d state electrons of the platinum and iridium respectively, and their PDOS decrease sharply in the energy region at -10 eV below the Fermi level. This reduction results in significant hybridization between metal 5d and H 1s electrons. This phenomenon is also found in other transition metal hydrides [30], in which the hybridization is suggested to be important for superconductivity. This hybridization also exists in the high pressure phase. However, on carefully examining the PDOS (Fig. 4 (a-b)) at the Fermi level, the hybridization between metal 5d and H 1s electrons in the NaCl phase seems to be stronger than that in the high pressure phase, implying the possibility of high Tc in the NaCl phase.

The charge density distribution for MH containing M+ and H- ion is shown in Fig. 5 (a-b). From the Fig. 5 (a-b), it is observed that the voids (i.e. charge depletion regions)

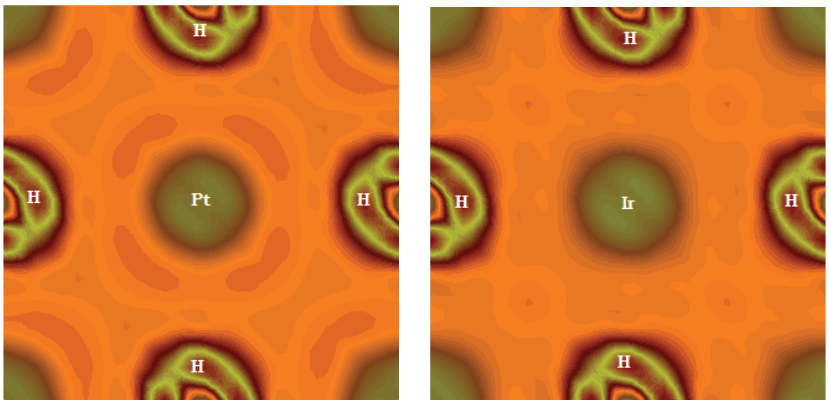

Figure 5: (a)Charge density distribution of PtH; (b)Charge density distribution of IrH.

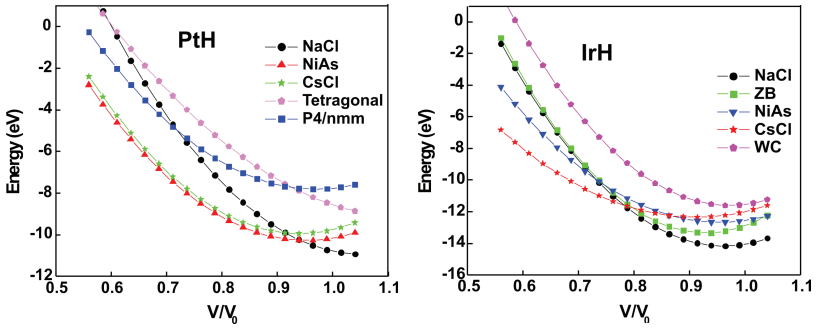

(a) (b)

Figure 6: (a)The total energies as a function of reduced volume for PtH; (b)The total energies as a function of reduced volume for IrH.

are narrow between H ions and broad between the metal ions. On increasing the M-ion atomic number the M-H bonding becomes stronger and these voids change their shape. It is also found that the light coloured areas indicate electron gain, whereas the darker areas indicate electron loss. Because the electron gain in hydrogen is much greater than that in the metal, the minimum and maximum values of electron gain and loss are truncated, in order to keep enough resolution around the metals. Electron gain on the hydrogen position is substantial, indicating that the hydrogen does not insert as a bare proton. Near the metal both regions of positive and negative charge difference exist, corresponding to the loss or gain of d occupation. Significant loss of d state electrons is observed, which is due to the formation of a bonding-antibonding pair between the direct overlapping of hydrogen s with metal d orbital. A more detailed understanding of *d* orbital's gain occupation can be obtained from the total density of states.

From Fig. 5 (a-b), it is also observed that the charge density around H atoms exhibit a strong directional distribution of metal atoms, indicating that the bonding between metal and H atoms is covalent in nature. The charge density distribution between metal and H atoms in the cubic structure is much denser than those in other structures. Thus, our results predict that the bonding in these hydrides is a mixture of metallic, covalent and ionic in attribution.

3.3 Structural phase transition under pressure

At normal pressure, Platinum hydride (PtH) and Iridium hydride (IrH) are highly stable in the rock salt structure. The total energy calculations are performed for five different phases of PtH and IrH, corresponding to the reduced volume of V/V_0=1.0-0.5 and the results are shown in Fig. 6 (a-b) respectively.

From the Fig. 6 (a-b), it is observed, at high pressure PtH transforms into hexagonal (NiAs) which agrees experimental result [14], where as IrH transforms into body centered cubic (CsCl) structure. Further from enthalpy calculation, the structural phase transition

from NaCl→NiAs is observed for PtH and from NaCl→CsCl structure for IrH.

The transition pressure value for the structural phase transition (P_t) is determined by calculating the Gibb's (G) free energies for the two phases, NaCl, NiAs for PtH and NaCl, CsCl for IrH

$$G = E_{tot} + PV - TS \tag{3}$$

Since the theoretical calculations are performed at $T = 0$K, the Gibbs free energy becomes equal to enthalpy. Then the equation (3) becomes

$$H = E_{tot} + PV \tag{4}$$

At a given pressure a stable structure is one for which the enthalpy has its minimum value and transition pressures are calculated at which the enthalpies of the two phases are equal. The enthalpy as a function of pressure is shown in inset of Fig. 7 (a-b).

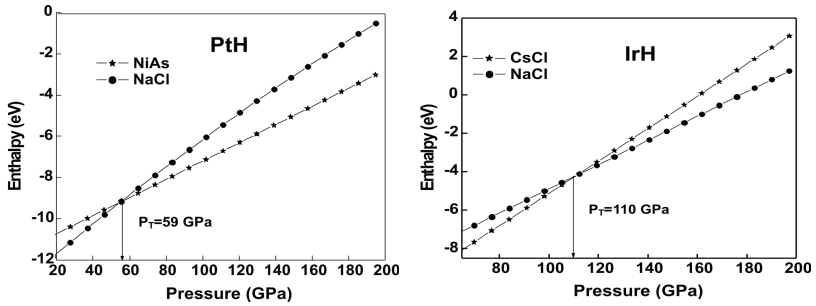

(a) (b)

Figure 7: (a)The enthalpy as a function of pressure for PtH; (b)The enthalpy as a function of pressure for IrH.

The phase transitions from NaCl-PtH to NiAs-PtH occur at 59 GPa and NaCl-IrH to CsCl-IrH occur at 110 GPa. A new high pressure CsCl phase is predicted for Iridium hydride.

3.4 Elastic properties

The elastic constants of solids provide a link between mechanical and dynamical behaviors of crystals, and give important information concerning the nature of forces operating in solids. In particular, they provide information on stability and stiffness of materials [31]. Thus, it is essential to investigate the elastic constants to understand the mechanical properties of PtH and IrH. Consider a symmetric 3×3 non-rotating strain tensor ε which has matrix elements ε_{ij} (i, j = 1, 2 and 3) defined by Eq. 5

$$\varepsilon_{ij} = \begin{pmatrix} e_1 & \frac{e_6}{2} & \frac{e_5}{2} \\ \frac{e_6}{2} & e_2 & \frac{e_4}{2} \\ \frac{e_5}{2} & \frac{e_6}{2} & e_3 \end{pmatrix} \tag{5}$$

Such a strain transforms the three lattice vectors defining the unstrained Bravais lattice a_K, K=1, 2 and 3) to the strained vectors { a'_K, K=1, 2 and 3} as given by

$$a'_K = (I+\varepsilon)a_K \tag{6}$$

where I is defined by its elements, $I_{ij}=1$ for $i=j$ and 0 for $i\neq j$. Each lattice vector a_K or a'_K is a 3×1 matrix. The change in total energy due to the above strain (5) is

$$\Delta E = \frac{E(\{e_i\})-E_0}{V_0} = \Big(1-\frac{V}{V_0}\Big)P(V_0)+\frac{1}{2}\Big(\sum_1^6\sum_1^6 C_{ij}e_ie_j\Big)+O(\{e_i^3\}) \tag{7}$$

where V_0 is the volume of the unstrained lattice, E_0 is the total minimum energy at this unstrained volume of the crystal, $P(V_0)$ is the pressure of the unstrained lattice, and V is the new volume of the lattice due to strain in Eq. (5). In Eq. (7), $C_{ij}=C_{ji}$ due to crystal symmetry. This reduces the elastic constants from 36 to 21. Further crystal symmetry reduces the number to 5 ($C_{11}, C_{12}, C_{44}, C_{13}, C_{33}$) for hexagonal crystals and 3(C_{11}, C_{12}, C_{44}) for cubic crystals. A proper choice of the set of strains $\{e_i, i=1,2,\cdots,6\}$, in Eq. (7) leads to a parabolic relationship between $\Delta E/V_0$ ($\Delta E \equiv E-E_0$) and the chosen strain. Such choices of the set $\{e_i\}$ and the corresponding form of ΔE for cubic [32] and hexagonal [33] lattices are given in Table 4 and Table 5 respectively.

Table 4: Strain combinations in the strain tensor Eq. (5) for calculating the elastic constants of cubic structures (rock salt and CsCl).

Strain	Parameters (unlisted $e_i=0$)	$\Delta E/V_0$
1	$e_1=e_2=\delta, e_3=(1+\delta)^{-2}-1$	$3(C_{11}-C_{12})\delta^2$
2	$e_1=e_2=e_3=\delta$	$(3/2)(C_{11}+2C_{12})\delta^2$
3	$e_6=\delta, e_3=\delta^2(4-\delta^2)^{-1}$	$(1/2)C_{44}\delta^2$

The elastic properties of normal and high pressure phases are studied. We strained the lattice by 0%, ±1%, and ±2% to obtain the total minimum energies $E(V)$ at these

Table 5: Strain combinations in the strain tensor Eq. (5) for calculating the elastic constants of hexagonal structure (NiAs).

Strain	Parameters (unlisted $e_i=0$)	$\Delta E/V_0$
1	$e_1=\delta$	$(1/2)C_{11}\delta^2$
2	$e_3=\delta$	$(1/2)C_{33}\delta^2$
3	$e_4=\delta$	$(1/2)C_{44}\delta^2$
4	$e_1=e_2=\delta$	$(C_{11}+C_{12})\delta^2$
5	$e_1=e_3=\delta$	$(1/2)(C_{11}+C_{33}+2C_{13})\delta^2$

Table 6: Calculated elastic constants C_{11}, C_{12}, C_{44}, C_{13}, C_{33} (GPa), Young's modulus E (GPa), shear modulus G(GPa), B/G ratio and Poisson's ratio v.

	PtH		IrH	
	NaC1 (0 GPa)	NiAs (59 GPa)	NaC1 (0 GPa)	CsC1 (110 GPa)
C_{11}	481	448	462	453
C_{12}	197	165	179	174
C_{44}	106	80	72	76
C_{13}	-	53	-	-
C_{33}	-	374	-	-
B_0	294	259 301[16]	273	267
E	317	232	202	269
G	120	150	100	101
v	0.2905	0.2572	0.2792	0.2775
B/G	2.45	1.72	2.73	2.64

strains. These energies and strains were fitted with the corresponding parabolic equations of $\Delta E/V_0$ as given in Table 4 and 5 to yield the required second-order elastic constants. While computing these energies all atoms are allowed to relax with the cell shape and volume fixed by the choice of strains $\{e_i\}$. The calculated single crystal elastic constants C_{ij} (GPa), Young's modulus E(GPa), shear modulus G (GPa), Poisson's ratio (v), B/G ratio of PtH and IrH at ambient pressure are given in Table. 6. The bulk modulus is inversely proportional to the bond length, the smaller atomic size and shorten bond length can cause the bulk modulus to be larger and consequently the elastic constants.

The bulk modulus B_0 (GPa) and shear modulus G (GPa) for cubic and hexagonal crystal are calculated using the Voigt Reuss-Hill (VRH) approximation [34-36].

The Voigt average for the Bulk modulus of the cubic and hexagonal systems is given respectively as:

$$B_0 = \frac{(C_{11}+2C_{12})}{3} \tag{8}$$

$$B_0 = \frac{2}{9}\left[C_{11}+C_{12}+2C_{13}+(1/2)C_{33}\right] \tag{9}$$

The Voigt average for the shear modulus of the cubic and hexagonal systems is given respectively as:

$$G = \frac{3C_{44}+C_{11}-C_{12}}{5} \tag{10}$$

$$G = \frac{2(C_{11}+C_{33})}{15} - \frac{(C_{12}+2C_{13})}{15} + \frac{3\left(2C_{44}+(1/2)(C_{11}-C_{12})\right)}{15} \tag{11}$$

The strain energy $1/2C_{ij}e_ie_j$ of a given crystal in Eq. (5) must always be positive for all possible values of the set $\{e_i\}$; otherwise the crystal would be mechanically unstable. For a stable cubic structure, the three independent elastic constants C_{ij} (C_{11}, C_{12} and C_{44}) should satisfy the well known Born-Huang criteria for the stability of cubic crystals [37].

$$C_{44}>0,\ C_{11}>|C_{12}|,\ C_{11}+2C_{12}>0 \tag{12}$$

while for a hexagonal crystal, the five independent elastic constants C_{ij} (C_{11}, C_{12}, C_{33}, C_{13}, C_{44}) should satisfy the well known Born-Huang criteria for stability [37]

$$C_{12}>0,\ C_{33}>0,\ C_{11}>C_{12},\ C_{44}>0 \tag{13}$$

$$(C_{11}+C_{12})C_{33}>2C_{13}^2 \tag{14}$$

Clearly, the calculated elastic constants for cubic and hexagonal PtH and IrH satisfy Born-Huang criteria, suggesting that they are mechanically stable.

Young's modulus (E) is calculated in terms of the computed data using the following relation:

$$E=\frac{9BG}{(3B+G)} \tag{15}$$

Bulk modulus (B_0) and shear modulus (G) can measure the resistance of a material to volume and shape change respectively. From Table 6, it is seen that both PtH and IrH are more inclined to resist with volume change than shape change. Young's modulus is often used to provide a measure of stiffness of a solid, i.e., larger the value of Young's modulus, stiffer is the material. Among these hydrides cubic PtH is stiffer than IrH. Poisson's ratio is associated with the volume change during uniaxial deformation, which is expressed as in Eq. (16) for cubic and Eq. (17) for hexagonal crystals

$$v=\frac{C_{12}}{C_{11}+C_{12}} \tag{16}$$

$$v=\frac{3B-2G}{6B+2G} \tag{17}$$

During elastic deformation no volume change occurs, If $v=0.5$ and the material is incompressible. The low v value means that a large volume change is associated with its deformation. In addition, Poisson's ratio provides more information about the characteristics of the bonding forces than any of the other elastic constants. Among the PtH and IrH, the Poisson's ratio of cubic IrH is lower than PtH, indicating that the Ir-H bonding is more directional. The ratio of bulk modulus to shear modulus is used to estimate the brittle or ductile behavior of materials. A high B/G value is associated with ductility, while a low B/G value corresponds to brittle nature. The critical value which separates ductile and brittle materials is about 1.75. From Table 6, it is found that NaCl- PtH and IrH are brittle in nature.

3.5 Superconductivity of PtH and IrH

The continuous promotion of s electron to d shell in solids is one of the factors which induce superconductivity. In the PtH and IrH, the d - electron number increases as a function of pressures ranging from normal to high pressure. This leads to the improvement of superconducting transition temperature (T_c) value. Therefore, the interaction between the conduction electrons and phonons increases and electron - Phonon coupling constant factor λ_{e-ph} also increases. This determines the superconducting nature of a compound. The calculated T_c values depend more sensitively on λ rather than θ_D (p) and μ^*. For various pressures, the superconducting transition temperature is estimated by using the McMillan equation modified by Allen and Dynes [38],

$$T_c = \frac{\omega_{\log}}{1.2} \exp\left[\frac{-1.04(1+\lambda)}{\lambda-\mu^*(1+0.62\lambda)}\right] \tag{18}$$

where λ is the electron- phonon coupling constant, μ^* is the electron - electron interaction parameter and $\omega_{\log}$ is the average phonon frequency. The average of the phonon frequency square is,

$$<\omega \log^2> = 0.5\theta_D^2 \tag{19}$$

The above expression gives a good estimate of the T_c value.

The variation of θ_D with pressure in terms of 'E_F' and the lattice constant 'a' is given as,

$$\theta_D(P) = \frac{\sqrt{E_F}}{\sqrt{E_F^0}} \frac{a_0}{a} \theta_D \tag{20}$$

But, in this case θ_D is taken as constant for various pressures. θ_D, a^0 and E_F^0 are Debye temperature, lattice constant and Fermi energy corresponding to normal pressure. The electron - phonon coupling constant λ can be written as [39]

$$\lambda = \frac{N(E_F) < I^2 >}{M < \omega^2 >} \tag{21}$$

where N (E_F) is the density of states at the Fermi energy. M is the atomic mass. $< I^2 >$ is the square of the electron - phonon matrix element averaged over the Fermi energy. $< I^2 >$ (in Rydbergs) can be written as [40],

$$< I^2 > = 2 \sum_i \left\{ \frac{(l+1)}{(2l+1)(2l+3)} \right\} M_{l,l+1}^2 \left\{ \frac{N_l(E_F) N_{l+1}(E_F)}{N(E_F)^2} \right\} \tag{22}$$

where $M_{l,l+1}$ are the electron-phonon matrix elements which can be expressed in terms of the logarithmic derivatives.

$$D_l = \frac{d \ln \phi_l}{d \ln r}\Big|_{r=s} \tag{23}$$

Table 7: Estimated superconducting transition temperature T_c (K), electron-phonon coupling constant λ, electron-electron interaction parameter μ^* and debye temperature (K).

Element	Pressure (GPa)	λ	μ^*	ω_{log}	T_c (K)
PtH	0	0.5393	0.0739	211	8.58
	33	0.79838	0.06523	282	16.32
	89	0.86987	0.05847	346	23.82
IrH	0	0.3717	0.17317	304	5.67
	28	0.62162	0.16021	386	6.29
	75	0.72169	0.15433	456	10.06

is evaluated at the sphere boundary,

$$M_{l,l+1} = -\phi_l \phi_{l+1}[(D_l(E_F)-1)(D_{l+1}(E_F)+l+2)+(E_F-V(S))S^2] \tag{24}$$

where ϕ_l is the radial wave function at the muffin-tin sphere radius corresponding to the Fermi energy. The logarithmic derivative of the radial wave function at the sphere boundary (D_l), the muffin-tin potential at the sphere boundary $(V(S))$ and the radius of the muffin-tin sphere (S) are taken from the output of TB-LMTO program.

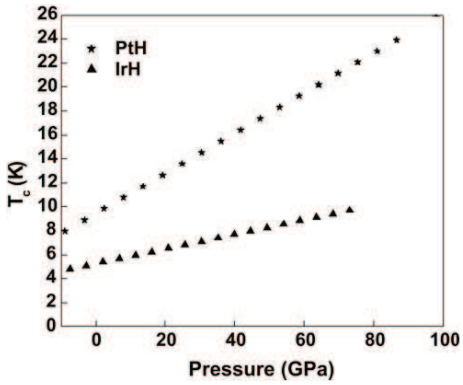

Figure 8: Superconducting transition temperature T_c of PtH and IrH as a function of pressure.

The electron - electron interaction parameter μ^* is estimated using the relation [41],

$$\mu^* = \frac{0.26N(E_F)}{(1+N(E_F))} \tag{25}$$

The T_C, μ^* and λ values are computed for PtH and IrH for various pressures and are given in the Table 7. The variation of T_C with pressure for PtH and IrH are plotted and is given in Fig. 8. From the Table 7, it is found that the Debye temperature increases with increase in pressure. Therefore the main reason for the increase in superconducting transition temperature is due to the increase in electron-phonon coupling constant (λ)

and electron-electron interaction parameter (μ^*) with pressure. The calculated maximum super conducting transition temperature for PtH and IrH are 23.8 K (87 GPa) and 10 K (110 GPa) respectively.

From the Fig. 8, it is also observed that the superconducting transition temperature of PtH increases with pressure up to 89 GPa and for IrH, superconducting transition temperature increases with pressure up to 75 GPa.

4 Conclusion

The structural, electronic and mechanical properties of PtH and IrH have been investigated using Vienna ab-initio simulation code. Our results suggest that cubic-NaCl structure is the most stable structure at ambient pressure, among the considered phases for both PtH and IrH. All the calculated elastic constants obey the Born-Huang criteria, suggesting that they are mechanically stable. It is observed that the bonding in NaCl PtH and IrH structure is a mixture of metallic, covalent, and ionic characters. A pressure induced structural phase transition from NaCl to NiAs and NaCl to CsCl is also predicted in PtH and IrH respectively. The maximum superconducting transition temperature achieved in platinum hydride and iridium hydride are 23.8K and 10K respectively.

Acknowledgments We thank our college management for their constant encouragement. The financial assistance from UGC (MRP.F.No.38-141/2009) is acknowledged.

References

[1] J. Garces and P. Vajda, Int. J. Hydrogen Energy 35 (2010) 6025.
[2] Y. Fukai, The Metal-Hydrogen System (Springer Verlag, Berlin, 2005).
[3] N. L. Rosi Science, 300 (2003) 1127.
[4] I. P. Jain, C. Lal, and A. Jain, Int. J. hydrogen Energy 35 (2010) 5133.
[5] M. Felderhoff and B. Bogdanovic, Int. J. Mol. Sci. 10 (2009) 325.
[6] X. J. Chen, C. Zhang, Y. Mang, R. Q. Zhang, H. Q. Lin, V. V. Struzhkin, and H. K.Mao, Phys. Rev. Lett. 106 (2011) 135502.
[7] L. S. Dubrovinsky, S. K. Saxena, F. Tutti, S. Rekhi, and T. Lebehan, Phys. Rev. Lett. 84 (2000) 1720.
[8] J. F. Lin, V. V.Struzhkin, S. D. Jacobsen, M. Y. Hu, P. Chow, J. Jung, J. Liu, H. K. Mao, and R. J. Hemley, Nature 436 (2005) 377.
[9] N. C. Holmes, J. A. Moriaty, G. R. Gathers, and W. J. Nellis, J. Appl. Phys. 66 (1989) 2962.
[10] M. I. Eremets, I. A. Trojan, S. A. Medvedev, J. S. Tse, and Y. Yao, Science 319 (2008) 1506.
[11] T. Matsuoka and K. Shimizu, Nature 458 (2009) 186.
[12] V. E. Antonov, J. Alloy. Comp. 110 (2002) 330.
[13] N. Hirao, F. Hiroshi, O. Yasuo, T. Kenichi, and K. Takumi, Acta Crystallogr. A 64 (2008) C609.
[14] T. Scheler, O. Degtyareva, M. Marques, C. L. Guillaume, J. E. Proctor, S. Evans, and E. Gregoryanz, Phys. Rev. B. 83 (2011) 214106.
[15] D. A. Papaconstantopoulos, J. Less. Common. Metals 73 (1980) 305.

[16] D. Y. Kim, R. H. Scheicher, C. J. Pickard, R. J. Needs, and R. Ahuja, Phys. Rev. Lett. 107 (2011) 117002.
[17] P. E. Blöchl, Phys. Rev. B 50 (1994) 17953.
[18] G. Kresse, Phys. Rev. B 59 (1999) 1758.
[19] G. Kresse, J. Hafner, Phys. Rev. B 47 (1993) 558 .
[20] G. Kresse and J. Furthmuller, Comput. Mater. Sci. 6 (1996) 15.
[21] J. P. Perdew an, S. Burke, Phys. Rev. Lett. 78 (1997) 1396.
[22] H. J. Monkhorst and J. D. Pack, Phys. Rev. B 13 (1976) 5188.
[23] W. Khon and L. Sham, Phys. Rev. A 140 (1965) 1133.
[24] H. L. Skriver, The LMTO Method (Springer, Heidelberg, 1984).
[25] O. K. Anderson, Phys. Rev. B 12 (1975) 3060.
[26] O. K. Anderson and O. Jepson, Phys.Rev.Lett. 53 (1984) 2571.
[27] O. K. Anderson, O. Jepson, and M. Sob, Lecture Notes, ed. M. Yussouff (Springer, Verlag, 1987).
[28] O. Jepson and O. K. Anderson, Solid. State. Commun. 9 (1984) 1763.
[29] H. Gou, L. Hou, J. Zhang, and F. Gao, Appl. Phys. Lett. 92 (2008) 241901.
[30] D. Y. Kim, R. H. Scheicher, and R. Ahuja, Phys. Rev. Lett. 103 (2009) 077002.
[31] J. F. Nye , Physical Properties of Crystals, Their Representation by Tensors and Matrices (Oxford Press, Oxford, 1957).
[32] M. Kalay, H. Kart, and T. Cagin, J. Alloy. Comp. 484 (2009) 431.
[33] G. Steinle-Neumann, L. Stixrude, and R. E. Cohen, Phys. Rev. B , 69 (2004) 219903.
[34] W. Voigt, A Determination of the Elastic Constants for Beta Quartz, Lehrbuch De Kristallphysik (Terubner, Leipzig, 1928).
[35] A. Reuss, Z. Angew, Math. Mech. 9 (1929) 49.
[36] R. Hill, Proc. Phys. Soc. London, Sec. A 65 (1952) 349.
[37] M. Born, K. Huang, Dynamical Theory of Crystal Lattices, (Clarendon, Oxford,1956).
[38] P. B. Allen and R. C. Dynes. Phys. Rev B 12 (1975) 905.
[39] W. L. McMillan, Phys. Rev. B 167 (1968) 331.
[40] H. L. Skriver and I. Mertig, Phys. Rev. B 32 (1985) 4431.
[41] K. H. Bennemann and J. K. Garland, in: Superconductivity in d and f- Band Metals, ed. D. H. iDouglass (American Institute of Physics, New York, 1971).